


NANO EXPRESS

Open Access



Sb₂S₃ Thickness-Related Photocurrent and Optoelectronic Processes in TiO₂/Sb₂S₃/P3HT Planar Hybrid Solar Cells

Fan Wu^{1,2*} , Rajesh Pathak², Lan Jiang¹, Weimin Chen¹, Chong Chen³, Yanhua Tong⁴, Tiansheng Zhang¹, Ronghua Jian¹ and Qiquan Qiao^{2*}

Abstract

In this work, a comprehensive understanding of the relationship of photon absorption, internal electrical field, transport path, and relative kinetics on Sb₂S₃ photovoltaic performance has been investigated. The n-i-p planar structure for TiO₂/Sb₂S₃/P3HT heterojunction hybrid solar cells was conducted, and the photon-to-electron processes including illumination depth, internal electric field, drift velocity and kinetic energy of charges, photo-generated electrons and hole concentration-related surface potential in Sb₂S₃, charge transport time, and interfacial charge recombination lifetime were studied to reveal the key factors that governed the device photocurrent. Dark *J-V* curves, Kelvin probe force microscope, and intensity-modulated photocurrent/photovoltage dynamics indicate that internal electric field is the main factors that affect the photocurrent when the Sb₂S₃ thickness is less than the hole diffusion length. However, when the Sb₂S₃ thickness is larger than the hole diffusion length, the inferior area in Sb₂S₃ for holes that cannot be diffused to P3HT would become a dominant factor affecting the photocurrent. The inferior area in Sb₂S₃ layer for hole collection could also affect the *V*_{oc} of the device. The reduced collection of holes in P3HT, when the Sb₂S₃ thickness is larger than the hole diffusion length, would increase the difference between the quasi-Fermi levels of electrons and holes for a lower *V*_{oc}.

Keywords: Solar cells, Sb₂S₃, Photocurrent, Optoelectronic processes

Introduction

Sb₂S₃ has been increasingly utilized for solid thin-film solar cells because of its moderate bandgap of 1.7 eV and an absorption coefficient of $1.8 \times 10^5 \text{ cm}^{-1}$ [1, 2]. Sb₂S₃ thin films can be prepared by various methods, including spray pyrolysis [3], electrodeposition [4], chemically deposition [5], and thermal vacuum evaporation technique [6]. In Sb₂S₃-based photovoltaic device, photoelectric conversion efficiency (PCE) has reached to 5.7–7.5% by improved technology and device design [1, 2, 7–10]. However, current efficiencies of solid-state devices still remain low compared to other photovoltaic devices, such as dye-sensitized solar cells [11] and perovskite solar cells [12]. At present, most of the works

usually focus on finding the best technology to get better optoelectronic performance in solid-state devices [7–10, 13–15]. In this regards, it is imperative to study the photoelectronic processes in Sb₂S₃-based solar cells for guiding the device design and optimization. This includes a comprehensive understanding of the balance among absorption, internal electrical field, and transport path, and relative kinetics on Sb₂S₃ photovoltaic performance, which is important to guide the optimization of the Sb₂S₃-based hybrid solar cells. In this work, the conventional TiO₂/Sb₂S₃/poly(3-hexylthiophene-2,5-diyl)(P3HT) n-i-p device structure was used to study the charge carrier generation and dissociation dynamic processes for different thicknesses of Sb₂S₃.

It is obvious that the different thickness of Sb₂S₃ in TiO₂/Sb₂S₃/P3HT n-i-p solar cells can change (i) the amount of photon harvesting, which influences the photon-generated electron/hole concentration; (ii) the magnitude of internal electrical field across the Sb₂S₃ layer, which influences the photon-generated electron/

* Correspondence: wufanjay@126.com; qiquan.qiao@sdsstate.edu

¹School of Sciences and Key Lab of Optoelectronic Materials and Devices, Huzhou University, Huzhou 313000, China

²Center for Advanced Photovoltaics, Department of Electrical Engineering and Computer Sciences, South Dakota State University, Brookings, SD 57007, USA

Full list of author information is available at the end of the article

hole drift; (iii) electron/hole transport distance to the respective electrode; and (iv) electron/hole recombination [16, 17]. However, the reason for the Sb_2S_3 thickness-dependent performance in n-i-p structure is still ambiguous, which has been simply attributed to the issues with bulk resistance, photon absorption, generation/recombination of charge carriers, and internal electric field [16–21], but the detailed and quantified analysis for the thickness-dependent photovoltaic parameters is not clear yet. To gain insight into the change of J_{sc} and V_{oc} upon the Sb_2S_3 thickness, $\text{TiO}_2/\text{Sb}_2\text{S}_3/\text{P3HT}$ n-i-p solar cells were fabricated (Fig. 1), and the thickness of Sb_2S_3 -related photon-generated electron and hole transport processes which result in the different photocurrents was studied in this work. Moreover, we introduced dynamic intensity-modulated photocurrent/photovoltage spectra (IMPS/IMVS) and Kelvin probe force microscope (KPFM) characterization to study photon-to-electron processes and investigate the key factors that governed the device performance in different thicknesses of Sb_2S_3 solar cells.

Methods

Reagents

Etched FTO-coated glass substrates were purchased from Huanan Xiangcheng Co., Ltd., China. SbCl_3 (99%), $\text{Na}_2\text{S}_2\text{O}_3$ (99%), and titanium diisopropoxide (75% in isopropyl alcohol) were purchased from Adamas-beta. P3HT was ordered from Xi'an Polymer Company, China, and Ag (99.999%) was ordered from Alfa.

Device Fabrication

The substrates were cleaned via ultrasonication in soap water, acetone, and isopropanol for 60 min each, followed by treatment with UV-ozone for 30 min. A thin layer of compact TiO_2 (0.15 M titanium diisopropoxide in ethanol) was spin coated at 4500 rpm for 60 s, followed by annealing at 125 °C for 5 min and 450 °C for 30 min. Deposition of Sb_2S_3 on the top of the TiO_2 thin layer was performed by a chemical bath deposition (CBD) method [5, 10, 22]. An acetone solution containing SbCl_3 (0.3 M) was added dropwise into $\text{Na}_2\text{S}_2\text{O}_3$

(0.28 M) with stirring in an ice bath (~ 5 °C). The FTO substrate was covered with a thin layer of TiO_2 and then suspended upside-down in the aqueous solution when the color of the solution changed to orange. After 1 h, 1.5 h, 2 h, and 3 h of the CBD process, a smooth and uniform amorphous Sb_2S_3 layer was deposited onto the TiO_2 -coated FTO substrates, and the sample was thoroughly rinsed with de-ionized water and dried under N_2 flow. The substrate was further annealed for 30 min in a glovebox (O_2 : 0.1 ppm, H_2O : 0.1 ppm) under an N_2 atmosphere. The fabrication of n-i-p heterojunction was completed by spin casting (1500 rpm for 60 s) of P3HT (15 mg/mL) film on top of Sb_2S_3 inside a glovebox (O_2 : 0.1 ppm, H_2O : 0.1 ppm) under an N_2 atmosphere. Finally, the MoO_3 (10 nm) and Ag (100 nm) electrode was deposited by evaporation through a shadow mask.

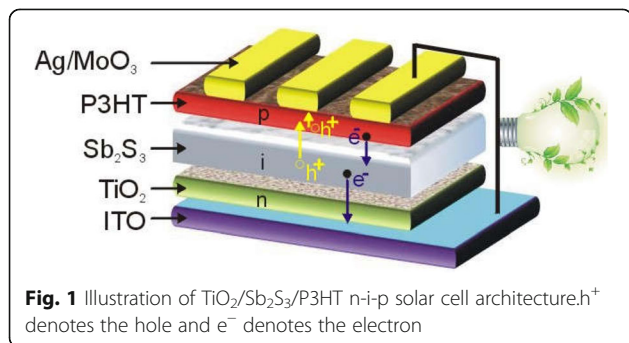
Instruments and Characterization

X-ray diffraction (XRD) patterns of the film were recorded by an MXP18AHF X-ray diffractometer with $\text{Cu K}\alpha$ irradiation ($\lambda = 1.54056$ Å). Scanning electron microscopy (SEM) measurements were performed on a field-emission scanning electron microscope (ZEISS, GeminiSEM 300). The absorption spectra were recorded with a Shimadzu UV-2600 spectrophotometer. Current density–voltage (J – V) characteristics were measured under AM 1.5 illumination with an intensity of 100 mW/cm^2 using a 94023A Oriel Sol3A solar simulator (Newport Stratford, Inc.). The light intensity from a 450 W xenon lamp was calibrated with a standard crystalline silicon solar cell. The J – V curves were collected using an Oriel I–V test station (Keithley 2400 Source Meter, Newport). External quantum efficiency (EQE) spectra of the solar cells were measured by using a QE/IPCE measurement kit (Zolix Instruments Co., Ltd.) in the spectral range of 300–900 nm. Intensity-modulated photocurrent spectra (IMPS) and intensity-modulated photovoltage spectra (IMVS) were measured using an electrochemistry workstation (IviumStat.h, Netherlands) under ambient conditions with a background intensity of 28.8 mW/cm^2 from a white light-emitting diode, with a small sinusoidal perturbation depth of 10%. Kelvin probe force microscope (KPFM) was performed by an Agilent SPM 5500 atomic force microscope equipped with a MAC III controller (comprising three lock-in amplifiers) to map the surface potential (SP).

Results and Discussion

Deposition and Characterization of $\text{Sb}_2\text{S}_3/\text{TiO}_2$ Film

FE-SEM images (Fig. 2a) clearly show that different thicknesses of Sb_2S_3 film are deposited on TiO_2 layer-coated glass substrates with the different CBD time t (1.0 h, 1.5 h, 2.0 h, 3.0 h). It can be seen that the uniform Sb_2S_3 layers were successfully obtained by CBD techniques. The average thickness of the Sb_2S_3 film estimated from the cross-



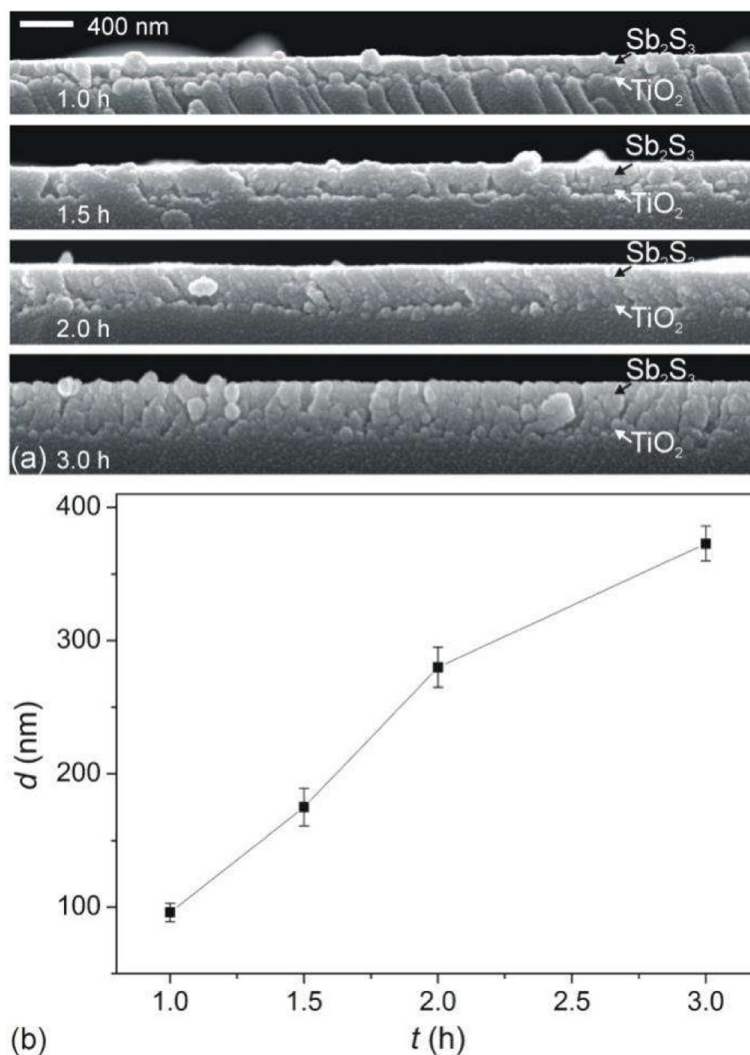


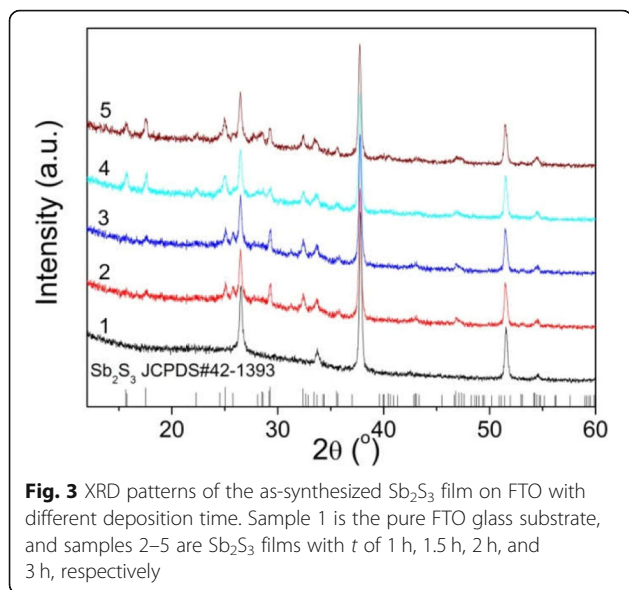
Fig. 2 **a** Cross-sectional FE-SEM images of Sb_2S_3 films on TiO_2 dense layer-coated glass substrates. **b** Average Sb_2S_3 thickness d plotted as a function of the CBD reaction time t for the Sb_2S_3 film deposition. The values were estimated by the FE-SEM cross-section images

sectional FE-SEM images is plotted in Fig. 2b as a function of the CBD time. The average thickness d of Sb_2S_3 film increases linearly with t (Fig. 2b). The average thickness increased almost linearly from 96 to 373 nm by changing CBD time from 1 to 3 h. The XRD patterns of Sb_2S_3 film with different thickness of Sb_2S_3 film on FTO glass are shown in Fig. 3. The measured XRD spectrum is indexed to orthorhombic Sb_2S_3 (JCPDS PCPDFWIN #42-1393) [23].

As shown in Fig. 4, the TiO_2 samples exhibit the absorption onset at 386 nm (3.21 eV) corresponding to the bandgap absorption of TiO_2 [24]. All the as-deposited $\text{TiO}_2/\text{Sb}_2\text{S}_3$ layers with different t of CBD exhibit an absorption edge at ca. 750 nm [25]. The absorption intensity of Sb_2S_3 on the TiO_2 surfaces is clearly in the order $3\text{ h} > 2\text{ h} > 1.5\text{ h} > 1\text{ h}$. This result also indicates that the Sb_2S_3 film gradually becomes thicker with a longer CBD t , which also agrees with the SEM results.

Solar Cells

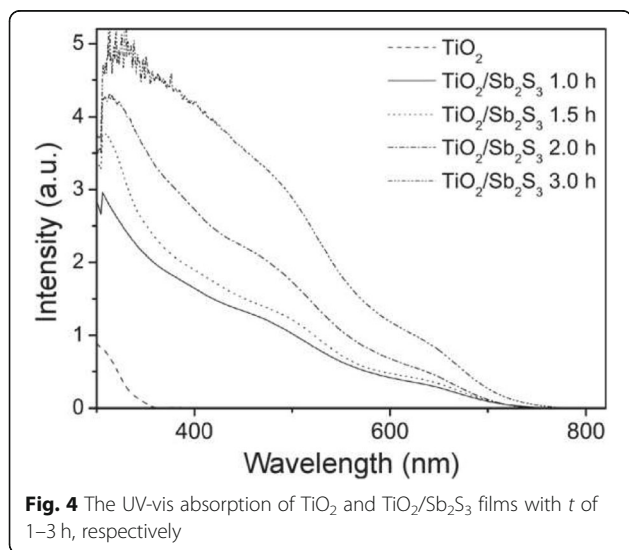
J - V characteristics of solar cells with different thickness d (i.e., CBD t) are compared in Fig. 5a. Table 1 presents the overall photovoltaic performance of these devices. Increasing thickness d (i.e., CBD time t) significantly affects device performance. The PCE increases as d increases from 96 to 175 nm (i.e., t increased from 1.0 to 1.5 h) and decreases thereafter, especially decreases largely after $d > 280$ nm (i.e., $t > 2$ h). Optimum Sb_2S_3 thickness of 175 nm can be determined by comparison of device efficiencies, at which point a maximum PCE of 1.65%, J_{sc} of 6.64 mA cm^{-2} , V_{oc} of 0.61 V, and FF of 40.81% can be achieved. This result is comparable to the other's reports [16, 26]. Liu et al. studied hybrid $\text{ZnO}/\text{Sb}_2\text{S}_3/\text{P3HT}$ n-i-p cells with Sb_2S_3 layers of three different thickness (50, 100, and 350 nm) by thermal evaporation achieving the highest PCE ($\sim 2\%$) with the



100-nm-thick Sb_2S_3 [12]. Kamruzzaman et al. studied $\text{TiO}_2/\text{Sb}_2\text{S}_3/\text{P3HT}$ n-i-p cells with Sb_2S_3 thicknesses of 45–120 nm by a thermal evaporation method, and the absorber Sb_2S_3 and hole transporting layer P3HT were annealed under atmospheric conditions. In their studies, the thickness of 100–120 nm showed a better power conversion efficiency of 1.8–1.94% [26]. Obviously, the thickness of Sb_2S_3 indeed strongly affects the device performance, even by different deposition strategies of Sb_2S_3 film or annealing condition.

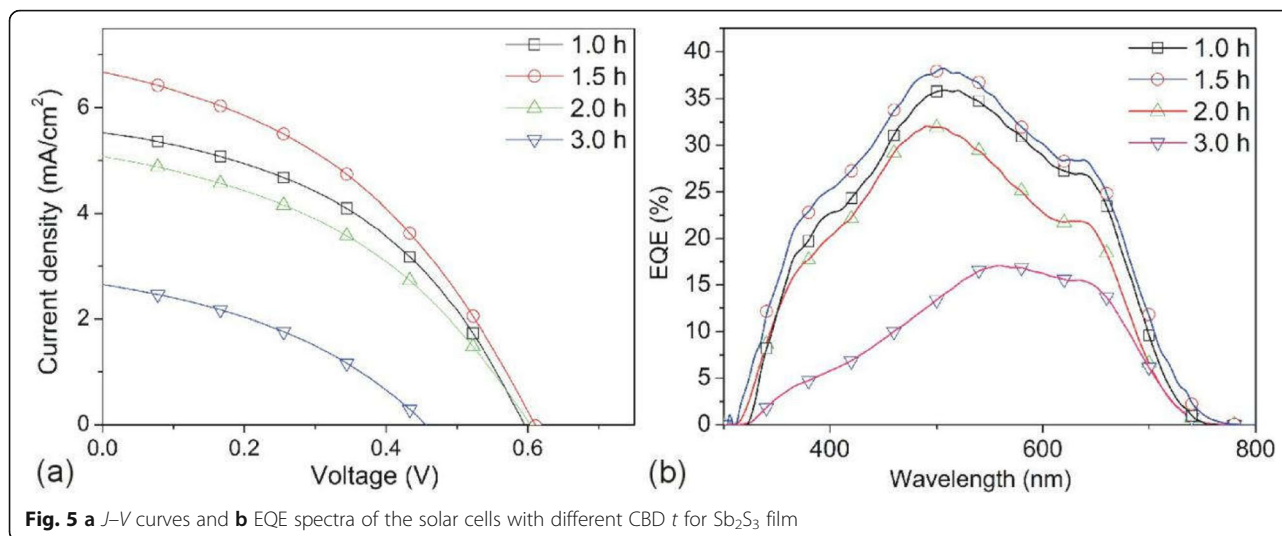
Charge Transport

The device J_{sc} increases remarkably with increasing Sb_2S_3 thickness d from 96 to 175 nm and then decreases



as the d increases (Fig. 5 and Table 1). The device J_{sc} is significantly dependent on the Sb_2S_3 thickness d . The charge carrier generation and dissociation are key processes for photocurrent generation. Firstly, visible light will pass through the TiO_2 layer due to its visible light window property (Fig. 4) and begin to be absorbed from $\text{TiO}_2/\text{Sb}_2\text{S}_3$ interface. Sb_2S_3 has been proved to be a high absorption coefficient α around 10^5 cm^{-1} in the visible region [27]. Here, we take $\alpha = 10^5 \text{ cm}^{-1}$ for Sb_2S_3 . The thickness-dependent illumination depth is depicted in Fig. 6 according to the Beer-Lambert law $I(x) = I_0 e^{-\alpha x}$, in which the I_0 is the incident photon flux and the $I(x)$ is the photon flux in Sb_2S_3 . Obviously, the incident photons cannot be absorbed fully when the Sb_2S_3 has a thickness of 100 nm or 200 nm (Fig. 6b). The d -related ratio of absorbed photon (N_a)/incident photons (N_i) can be calculated by integration of the area of the shaded area in coordinate. As shown in Fig. 6b (also refer Fig. 7b), the N_a/N_i is 61% when the $d = 96 \text{ nm}$ and N_a/N_i is enhanced to 82% when the $d = 175 \text{ nm}$. It can be believed that the further 21% photons absorbed might cause the increase in J_{sc} from 5.50 to 6.64 mA/cm^2 . When the d increases to 280 nm, the extra 11% photons are absorbed and the N_a/N_i is further enhanced to 93%, which shows that more photons could be further absorbed and then might generate more electrons. However, the device J_{sc} decreased to 5.06 mA/cm^2 which is lower than the case of $d = 96 \text{ nm}$. When the d increases to 373 nm, the N_a/N_i is close to 100%, and the device J_{sc} is sharply decreased to 2.64 mA/cm^2 . Therefore, absorption is not the sole factor that affects J_{sc} .

The semilogarithmic plots of the J - V curve of solar cells in the dark normally exhibit three distinct regimes: (i) linear increase for leakage dominated current, (ii) exponential increase for diffusion dominated current, and (iii) quadratic increase for space-charge-limited current. The built-in voltage (V_{in}) normally can be estimated at the turning point where the dark curve begins to follow a quadratic behavior (Fig. 7a). Dependences of V_{in} , J_{sc} , N_a/N_i , E_{ke} , and E_{kh} on CBD t are shown in Fig. 7b. When d increased from 96 to 175 nm, the N_a/N_i enhanced 34.44%; however, the J_{sc} only increased by 20.72%, which means that there is another factor limiting the J_{sc} increment. It has been inferred that this was might due to the decreased internal electrical field across the Sb_2S_3 layer, which weakened the photon-generated electron/hole drift [16]. Therefore, we calculated the internal electrical field E_{in} cross the Sb_2S_3 based on the relation of $E_{\text{in}} = V_{\text{in}}/d$ (Table 2). Moreover, the drift velocity of electron v_e and hole v_h , kinetic energy of electron E_{ke} , and hole E_{kh} under internal electric field E_{in} were also calculated (Table 2 and Fig. 7b). When the d is 96 nm, the E_{ke} is 296.56 meV, and E_{kh} is 53.25 meV. When the d increased to 175 nm, the E_{ke} largely



decreases to 95.29 meV and E_{kh} decreased to 17.12 meV, which is lower than the thermal energy at ambient temperature (E_{kt} , 26 meV). This result indicates that the internal electric field has little effects on hole drift when Sb_2S_3 thickness is or larger than 175 nm. Obviously, the reduced E_{ke} and E_{kh} with the thicker Sb_2S_3 should be the reason that limits the increment of J_{sc} . Further increasing d from 175 to 280 nm, the $N_{\text{a}}/N_{\text{i}}$ enhanced to 13.84%; however, the J_{sc} get decreased. This might be due to the decrease in E_{ke} which is close to the E_{kt} ($d = 280$ nm) but much lower than the E_{kh} ($d = 373$ nm), which means the E_{in} gradually has little effects on electron drift when $d > 280$ nm as observed in this work. Therefore, E_{in} decrement-related electron drift might be responsible for the J_{sc} reduction when d increased from 175 to 280 nm. However, when the d increased to 373 nm, the E_{in} has little effects on electron and hole drift, but J_{sc} still largely decreased, which indicates that E_{in} is also not the sole factor that affects the J_{sc} .

We used KPFM to characterize the photo-generated electrons and hole concentration-related surface potential (SP) in $\text{Sb}_2\text{S}_3/\text{P3HT}$. The sample for the KPFM measurement was prepared by drop casting the P3HT precursor solution onto part of the $\text{FTO}/\text{TiO}_2/\text{Sb}_2\text{S}_3$ film surface (Fig. 8). As the Sb_2S_3 thickness increases from 96 to 373 nm, the SP on the top of Sb_2S_3 gradually becomes smaller, which means the Fermi level on the

Sb_2S_3 surface becomes lower [28]. This demonstrates that electrons which could diffuse to the top surface are being gradually reduced, indicating that there is an inferior region for photo-generated electrons in thicker Sb_2S_3 film as shown in Fig. 6. We also examined the SP of P3HT part. The changes of SP of the P3HT are different from that of Sb_2S_3 . P3HT might be excited by light to generate excitons and then separate into electrons and holes [29, 30], when Sb_2S_3 is very thin (< 200 nm). When Sb_2S_3 becomes thicker, P3HT only acts as the hole transport layer, because most of the photons are absorbed by Sb_2S_3 (Fig. 3). Therefore, when the thickness of Sb_2S_3 is less 280 nm, P3HT could be photo-excited, resulting in the Fermi level of P3HT gradually decreases as Sb_2S_3 thickness gradually increases (decreased photo-exciton). In the case of 280 nm, the SP of P3HT drops rapidly, because there is no photo-exciton and the P3HT works just as a hole transport layer to collect holes. As the Sb_2S_3 thickness increases to 373 nm which is much larger than the hole transport length, the hole collection also drops rapidly, causing the Fermi level in P3HT to rise again. Moreover, the changes of SP in P3HT is much larger than that in the Sb_2S_3 in the case of $d = 373$ nm, which means that hole collection is worse than electron collection and therefore would probably lead to a much decreased J_{sc} .

Table 1 Device performance of the $\text{TiO}_2/\text{Sb}_2\text{S}_3/\text{P3HT}$ n-i-p planar solar cells under AM 1.5 illumination of $100 \text{ mW}/\text{cm}^2$

CBD time (h)	Thickness d (nm)	V_{oc} (V)	J_{sc} (mA cm^{-2})	FF (%)	PCE (%)	τ_{IMPS} (μs)	τ_{IMVS} (ms)
1.0	96	0.59	5.50	43.93	1.44	5.04	1.01
1.5	175	0.61	6.64	40.81	1.65	5.52	1.01
2.0	280	0.60	5.06	40.87	1.25	6.34	1.01
3.0	373	0.46	2.64	37.56	0.45	6.64	1.01

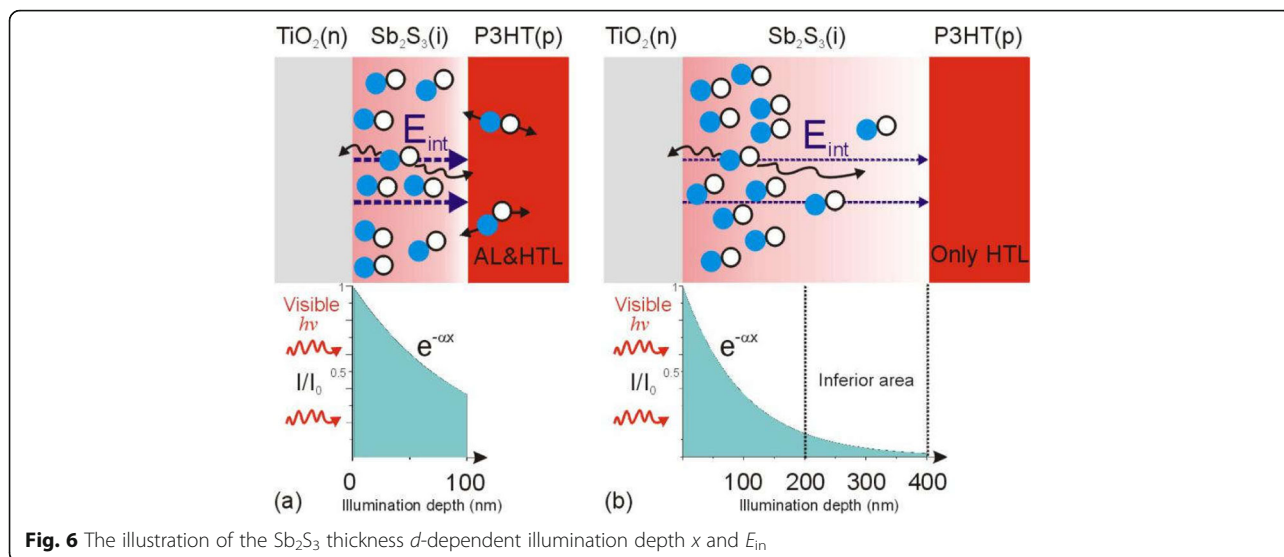


Fig. 6 The illustration of the Sb_2S_3 thickness d -dependent illumination depth x and E_{in}

Furthermore, IMPS and IMVS, as the powerful dynamic photoelectrochemical methods in dye-sensitized solar cells [31] and perovskite solar cells [32], have been applied to study the charge transport dynamics in this work. IMPS/IMVS measures the photocurrent/photovoltage response to a small sinusoidal light perturbation superimposed on the background light intensity under short-circuit/open-circuit condition [31–33]. The measured IMPS or IMVS responses appear in the fourth quadrant of the complex plane with a shape of the distorted semicircle (Fig. 10a, b). The time constant τ defined by the frequency (f_{min}) of the lowest imaginary component of IMPS or IMVS response is an evaluation of the transit time τ_{IMPS} for the electrons to reach the collection electrode under short-circuit condition or the electron

lifetime τ_{IMVS} related to interfacial charge recombination under open-circuit condition. According to the relation $\tau = (2\pi f)^{-1}$ [31–35], τ_{IMPS} and τ_{IMVS} in the devices were calculated (Table 1). The increased τ_{IMPS} suggests a longer transport path of charges to collection electrode, whereas the unchanged τ_{IMVS} infers the same interfacial charge recombination [33]. The interfacial charge collection efficiency η_c is typically considered as $\eta_c = 1 - \tau_{IMPS}/\tau_{IMVS}$ [31–35]. Obviously, the longer transport time of the τ_{IMPS} and the short interfacial charge recombination lifetime of the τ_{IMVS} would cause a worse charge collection and vice versa. In this study, the τ_{IMPS} increases with the thicker Sb_2S_3 while the τ_{IMVS} is unchanged. Therefore, interfacial charge collection efficiency η_c decreases with the thicker Sb_2S_3 , and the changes of J_{sc} in different

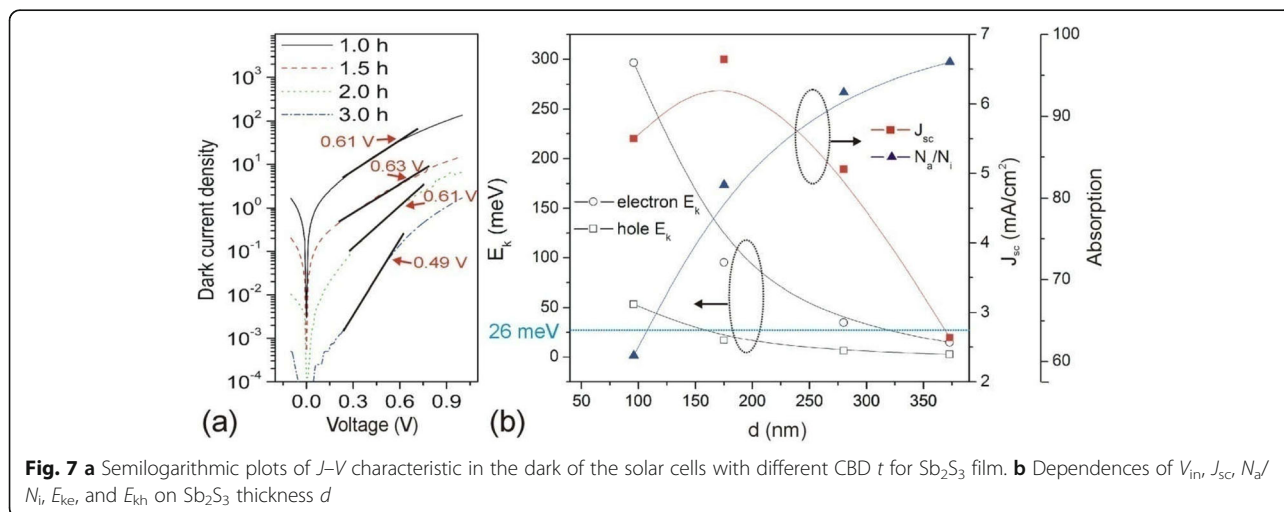


Fig. 7 **a** Semilogarithmic plots of J - V characteristic in the dark of the solar cells with different CBD t for Sb_2S_3 film. **b** Dependences of V_{inv} , J_{sc} , N_a/N_d / N_i , E_{ke} , and E_{kn} on Sb_2S_3 thickness d

Table 2 Parameters of V_{in} , internal electric field E_{in} , drift velocity of the electron (v_e) and hole (v_h), and kinetic energy of the electron (E_{ke}) and hole (E_{kh}) in the dark of the solar cells with different CBD t

d (nm)	V_{in} (V)	E_{in} ($\times 10^4$ Vcm $^{-1}$)	v_e (cm s $^{-1}$)	E_{ke} (meV)	v_h (cm s $^{-1}$)	E_{kh} (meV)
96	0.61	6.35	42.55	296.56	16.51	53.25
175	0.63	3.60	24.12	95.29	9.36	17.12
280	0.61	2.18	14.61	34.96	5.67	6.28
373	0.49	1.31	8.78	12.63	3.67	2.26

The mean value of d for a certain Sb_2S_3 deposition time t is used for calculation of the above parameters E_{in} , v_e , v_h , E_{ke} , and E_{kh}

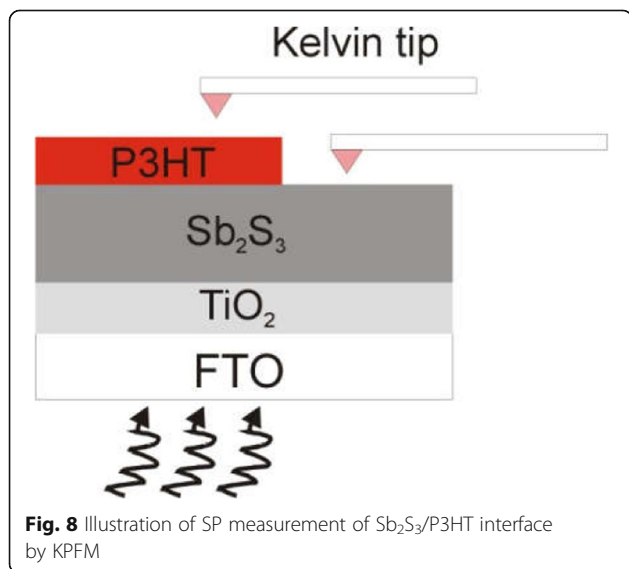
thickness of Sb_2S_3 solar cells should be caused by the transport path and charge collection efficiency, not by charge recombination.

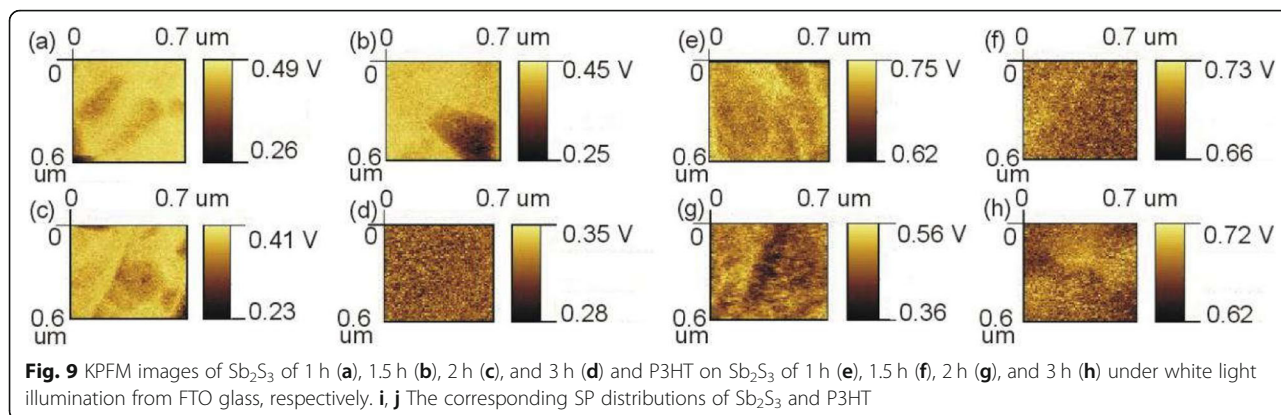
The increase in Sb_2S_3 thickness could absorb more photons which could enhance the photocurrent. However, in thicker Sb_2S_3 layer, most of electrons and holes are generated near the TiO_2 side due to exponential photon absorption (Fig. 10c); therefore, the transport path of most of the electrons are almost the same. However, most of the holes need to be diffused in a longer path than electrons in the thicker Sb_2S_3 layer, which is demonstrated by longer τ_{IMPS} in Fig. 10d. When the thickness exceeds the hole diffusion length, the inferior area in Sb_2S_3 for an inefficient hole generation and transport would decrease the photocurrent and weaken the J_{sc} and EQE. The hole diffusion length in Sb_2S_3 is around 180 nm [18]. When the thickness of Sb_2S_3 exceeds hole diffusion length, the collection performance of holes is reduced which is also responded by EQE spectra (Fig. 5b) since the absorption coefficient of the long wave is much lower than the short wave, resulting in a longer illumination depth for long wave (Fig. 9) [35]. Photo-

generated holes from long band could distribute more uniform in Sb_2S_3 than that from short band (photo-generated holes from short band could close to TiO_2 side), resulting in a more efficient collection of the hole from long band. Therefore, the EQE in long-wavelength part did not get a large decreased as much as short-wave part with Sb_2S_3 thickness of 373 nm (Fig. 5b).

As shown in Fig. 10d, it is easily understood that a smaller τ_{IMPS} is accompanied by a thinner Sb_2S_3 (i.e., a shorter charge transport path); however, τ_{IMVS} mainly remains the same when Sb_2S_3 thickness increased from 96 to 373 nm in this experiment, which means that there is no direct dependence of J_{sc} and V_{oc} on τ_{IMVS} (i.e., interfacial recombination) when Sb_2S_3 thickness changes. It is well known that the V_{oc} of the $TiO_2/Sb_2S_3/P3HT$ solar cells is normally determined by the difference between the quasi-Fermi levels of the electrons in the TiO_2 and the holes in the P3HT [36]. As the collection of holes is reduced in P3HT when the thickness of Sb_2S_3 is larger than the hole diffusion length, it would increase the difference between the quasi-Fermi levels of electrons and holes for a lower V_{oc} . In addition, a thicker Sb_2S_3 would increase the higher series resistance and worse charge collection efficiency; these unfavorable factors may cause a lower FF in thicker Sb_2S_3 device.

Although, the efficiency of planar $TiO_2/Sb_2S_3/P3HT$ n-i-p solar cells is very low, and how to further improve the device efficiency is a challenge. However, our results still demonstrated that some further improvements could be carried out. For example, enhancing the built-in electric field by employing some different electron transport layer or hole transport layer could enhance charge transport and collection. Moreover, how to improve the hole diffusion ability should be considered; maybe some conductive additives is helpful. In addition, interfacial engineer is also important for improving charge transfer and dissociation. Last but not least, the method that expressed in this paper might be offering some helpful reference for other relative high-efficiency solar cells (e.g., organic solar cells, perovskite solar cells).

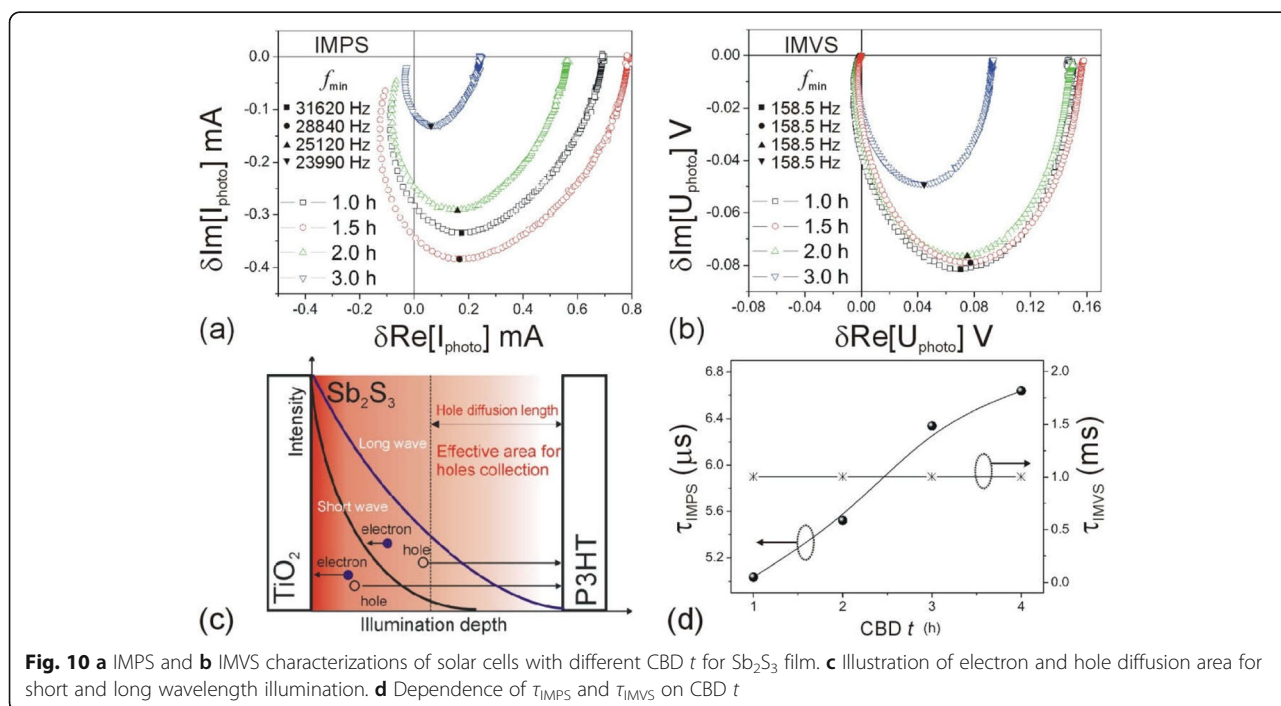




Conclusion

In this paper, the mechanism of photocurrent changes in $\text{TiO}_2/\text{Sb}_2\text{S}_3/\text{P3HT}$ n-i-p solar cells with different thickness of Sb_2S_3 was studied. When the thickness is less than the hole transport length, the absorption and internal electric field are the main factors that affect the photocurrent; when the thickness is larger than the hole transport length, the inferior area in Sb_2S_3 for an inefficient hole generation and transport is the main reason for photocurrent decrement. Results showed that device short-circuits' current density (J_{sc}) is increased with the enhanced photon absorption when the Sb_2S_3 thickness is less than the hole transport length; however, when the Sb_2S_3 thickness is larger than the hole transport length, device J_{sc} is sharply decreased with further increased absorption. Internal electric field decrement-related electron drift could

lead to the reduction in the J_{sc} when the thickness of Sb_2S_3 is less than the hole transport length. However, when the thickness of Sb_2S_3 is larger than the hole transport length, the internal electric field has little effects on electron and hole drift, but J_{sc} still largely decreased. KPFM and IMPS/IMVS characterization demonstrated that there is an inferior region for photo-generated electrons in thicker Sb_2S_3 film. The inferior area in Sb_2S_3 for a reduction of holes that can diffuse into the P3HT when the Sb_2S_3 thickness is larger than the hole diffusion length, leading to the obviously decreased J_{sc} . Moreover, the reduced collection of holes in P3HT with the increased thickness of Sb_2S_3 would increase the difference between the quasi-Fermi levels of electrons and holes for a lower V_{oc} .



Abbreviations

CBD: Chemical bath deposition; E_{in} : Internal electric field; E_{ke} : Kinetic energy of the electron; E_{kh} : Kinetic energy of the hole; E_{kt} : Thermal energy at ambient temperature; EQE: External quantum efficiency; FF: Fill factor; IMPS: Intensity-modulated photocurrent spectra; IMVS: Intensity-modulated photovoltage spectra; $J-V$: Current density–voltage; J_{sc} : Short-circuit current; KPFM: Kelvin probe force microscope; N_a : Absorbed photon; N_i : Incident photons; P3HT: Poly (3-hexylthiophene-2,5-diyl); PCE: Photoelectric conversion efficiency; SEM: Scanning electron microscopy; SP: Surface potential; UV-vis: Ultraviolet-visible spectroscopy; v_e : Drift velocity of the electron; v_h : Drift velocity of the hole; V_{in} : Built voltage; V_{oc} : Open-circuit voltage; XRD: X-ray diffraction

Acknowledgements

This work was supported by the National Natural Science Foundation of China (21607041, 11747312, 11647306), China Scholarship Council (201708330103), Science and Technology Planning Project of Zhejiang Province, China (2017C33240), and Zhejiang Provincial Natural Science Foundation of China (LQ14F040003). The authors also acknowledge the support provided under the “1112 Talents Project” of Huzhou city.

Authors' Contributions

FW carried out the experiments. FW and RP drafted the manuscript. LJ and WC participated in the device preparation. TH, TS, RJ, and CC participated in the design of the study. QQ conceived of the study and helped to draft the manuscript. All authors read and approved the final manuscript.

Competing Interests

The authors declare that they have no competing interests.

Author details

¹School of Sciences and Key Lab of Optoelectronic Materials and Devices, Huzhou University, Huzhou 313000, China. ²Center for Advanced Photovoltaics, Department of Electrical Engineering and Computer Sciences, South Dakota State University, Brookings, SD 57007, USA. ³Henan Key Laboratory of Photovoltaic Materials and School of Physics and Electronics, Henan University, Kaifeng 475004, China. ⁴Department of Materials Chemistry, Huzhou University, Huzhou 313000, China.

Received: 23 July 2019 Accepted: 23 September 2019

Published online: 16 October 2019

References

- Deng H, Zeng Y, Ishaq M, Yuan S, Zhang H, Yang X, Hou M, Farooq U, Huang J, Sun K, Webster RWH, Chen Z, Yi F, Song H, Hao X, Tang J (2019) Quasiepitaxy strategy for efficient full-inorganic Sb_2S_3 solar cells. *Adv Funct Mater*. <https://doi.org/10.1002/adfm.201901720>
- Kondrotas R, Chen C, Tang J (2018) Sb_2S_3 solar cells. *Joule* 2:857–878
- Kriisa M, Krunks M, Acik IO, Kärber E, Mikli V (2015) The effect of tartaric acid in the deposition of Sb_2S_3 films by chemical spray pyrolysis. *Mater Sci Semicond Process* 40:867–872
- Hong JY, Lin LY, Li X (2018) Electrodeposition of Sb_2S_3 light absorbers on TiO_2 nanorod array as photocatalyst for water oxidation. *Thin Solid Films* 651:124–130
- Li SA, Zhang Y, Tang R, Wang X, Zhang T, Jiang G, Liu W, Zhu C, Chen T (2018) Aqueous-solution-based approach towards carbon-free Sb_2S_3 films for high efficiency solar cells. *ChemSusChem* 11:3208–3214
- Yuan S, Deng H, Yang X, Hu C, Khan J, Ye W, Song H (2017) Postsurface selenization for high performance Sb_2S_3 planar thin film solar cells. *Acs Photonics* 4:2862–2870
- Tang R, Wang X, Jiang C, Li S, Jiang G, Yang S, Zhu C, Chen T (2018) Vacuum assisted solution processing for highly efficient Sb_2S_3 solar cells. *J Mater Chem A* 6:16322–16327
- Xu T, Qiao Q (2011) Conjugated polymer-inorganic semiconductor hybrid solar cells. *Energy Environ Sci* 4:2700–2722
- Zimmermann E, Pfadler T, Kalb J, Dorman JA, Sommer D, Hahn G, Weickert J, Schmidt-Mende L (2015) Toward high-efficiency solution-processed planar heterojunction Sb_2S_3 solar cells. *Adv Sci* 2:1500059
- Choi YC, Seok SI (2015) Efficient Sb_2S_3 -sensitized solar cells via single-step deposition of Sb_2S_3 using S/Sb-ratio-controlled $SbCl_3$ -thiourea complex solution. *Adv Funct Mater* 25:2892–2898
- Kweon DH, Baek JB (2019) Edge-functionalized graphene nanoplatelets as metal-free electrocatalysts for dye-sensitized solar cells. *Adv Mater* 31:1804440
- Jung EH, Jeon NJ, Park EY, Moon CS, Shin TJ, Yang TY, Noh JH, Seo J (2019) Efficient, stable and scalable perovskite solar cells using poly (3-hexylthiophene). *Nature* 567:511–515
- Yue W, Wei F, He C, Wu D, Tang N, Qiao Q (2017) L-Cysteine assisted-synthesis of 3D In_2S_3 for 3D $CuInS_2$ and its application in hybrid solar cells. *RSC Adv* 7:37578–37587
- Liu C, Qiu Z, Li F, Meng W, Yue W, Zhang F, Qiao Q, Wang M (2015) From binary to multicomponent photoactive layer: a promising complementary strategy to efficient hybrid solar cells. *Nano Energy* 12:686–697
- Yue W, Wu F, Liu C, Qiu Z, Cui Q, Zhang H, Gao F, Shen W, Han C, Qiao Q, Wang M (2013) $CuInS_2$ quantum dots incorporated ternary solar hybrid solar cells for higher efficiency with polymer-based hybrids for light-harvesting and straightforward oxide channels for electron transportation. *Sol Energy Mater Sol Cells* 114:43–53
- Liu CP, Wang HE, Ng TW, Chen ZH, Zhang WF, Yan C, Tang YB, Bello I, Martinu L, Zhang WJ, Jha SK (2012) Hybrid photovoltaic cells based on $ZnO/Sb_2S_3/P3HT$ heterojunctions. *Physica Status Solidi (b)* 249:627–633
- Christians JA, Kamat PV (2013) Trap and transfer. Two-step hole injection across the $Sb_2S_3/CuSCN$ interface in solid-state solar cells. *ACS Nano* 7:7967–7974
- Christians JA, Leighton DT, Kamat PV (2014) Rate limiting interfacial hole transfer in Sb_2S_3 solid-state solar cells. *Energy Environ Sci* 7:1148–1158
- Roelofs KE, Brennan TP, Bent SF (2014) Interface engineering in inorganic-absorber nanostructured solar cells. *J Phys Chem Lett* 5:348–360
- O'Mahony FT, Lutz T, Guijarro N, Gómez R, Haque SA (2012) Electron and hole transfer at metal oxide/ Sb_2S_3 /spiro-OMeTAD heterojunctions. *Energy Environ Sci* 5:9760–9764
- Choi YC, Lee DU, Noh JH, Kim EK, Seok SI (2014) Highly improved Sb_2S_3 sensitized-inorganic-organic heterojunction solar cells and quantification of traps by deep-level transient spectroscopy. *Adv Funct Mater* 24:3587–3592
- Chen W, Jiang L, Pathak R, Wu F (2019) Sb_2S_3/TiO_2 heterojunction solar cells based on carbon electrode with higher photocurrent. *ECS J Solid State Sci Technol* 8:Q67–Q71
- Yao S, Cui J, Huang JQ, Lu Z, Deng Y, Chong WG, Wu J, Haq MIU, Ciucci F, Kim JK (2018) Novel 2D Sb_2S_3 nanosheet/CNT coupling layer for exceptional polysulfide recycling performance. *Adv Energy Mater* 8:1800710
- De Mendonca VR, Ribeiro C (2011) Influence of TiO_2 morphological parameters in dye photodegradation: a comparative study in peroxo-based synthesis. *Appl Catal B Environ* 105:298–305
- Lee L, Park J, Han KS, Kumar RS, Sung MM (2019) Enhanced photovoltaic performance of Sb_2S_3 -sensitized solar cell using a novel Ni-4 mercaptophenol hybrid interfacial layer. *Appl Surf Sci* 476:897–904
- Kamruzzaman M, Chaoping L, Yishu F, Islam AFU, Zapfen JA (2016) Atmospheric annealing effect on $TiO_2/Sb_2S_3/P3HT$ heterojunction hybrid solar cell performance. *RSC Adv* 6:99282–99290
- Versavel MY, Haber JA (2007) Structural and optical properties of amorphous and crystalline antimony sulfide thin-films. *Thin Solid Films* 515:7171–7176
- Melitz W, Shen J, Kummel AC, Lee S (2011) Kelvin probe force microscopy and its application surf. *Sci Rep* 66:1–27
- Ravirajan P, Peiró AM, Nazeeruddin MK, Graetzel M, Bradley DD, Durrant JR, Nelson J (2006) Hybrid polymer/zinc oxide photovoltaic devices with vertically oriented ZnO nanorods and an amphiphilic molecular interface layer. *J Phys Chem B* 110:7635–7639
- Parize R, Katerski A, Gromyko I, Rapenne L, Roussel H, Kärber E, Appert E, Krunks M, Consonni V (2017) $ZnO/TiO_2/Sb_2S_3$ core-shell nanowire heterostructure for extremely thin absorber solar cells. *J Phys Chem C* 121:9672–9680
- Kant R, Chowdhury NR, Srivastav S (2019) Theory for IMPS on rough and finite fractal dye sensitized solar cell. *J Electrochem Soc* 166:H3047–H3064
- Ravishankar S, Aranda C, Sanchez S, Bisquert J, Saliba M, Garcia-Belmonte G (2019) Perovskite solar cell modeling using light and voltage modulated techniques. *J Phys Chem C* 123:6444–6449
- Klotz D, Ellis DS, Dotan H, Rothschild A (2016) Empirical in operando analysis of the charge carrier dynamics in hematite photoanodes by PEIS, IMPS and IMVS. *Phys Chem Chem Phys* 18:23438–23457
- Wu F, Qiao Q, Bahrami B, Chen K, Pathak R, Mabrouk S, Tong Y, Li X, Zhang T, Jian R (2018) Comparison of performance and optoelectronic

processes in ZnO and TiO₂ nanorod array-based hybrid solar cells. *Appl Surf Sci* 456:124–132

35. Li X, Wang Y, Tai M, Zhao X, Gu Y, Han J, Shen H, Li J, Lin H (2018) New insights into the origin of hysteresis behavior in perovskite solar cells. *Phys Chem Chem Phys* 20:16285–16293
36. Chang JA, Rhee JH, Im SH, Lee YH, Kim HJ, Seok SI, Nazeeruddin Md K, Gratzel M (2010) High-performance nanostructured inorganic-organic heterojunction solar cells. *Nano Lett* 10:2609–2612

Publisher's Note

Springer Nature remains neutral with regard to jurisdictional claims in published maps and institutional affiliations.

Submit your manuscript to a SpringerOpen[®] journal and benefit from:

- ▶ Convenient online submission
- ▶ Rigorous peer review
- ▶ Open access: articles freely available online
- ▶ High visibility within the field
- ▶ Retaining the copyright to your article

Submit your next manuscript at ▶ [springeropen.com](https://www.springeropen.com)
